JOURNAL OF GEOPHYSICAL RESEARCH, VOL. 113, C03S04, doi:10.1029/2007JC004197, 2008

Response of snow thermophysical processes to the passage of a polar low-pressure system and its impact on in situ passive microwave radiometry: A case study

A. Langlois,[1] T. Fisico,[1] D. G. Barber,[1] and T. N. Papakyriakou[1]

Received 4 March 2007; revised 28 January 2008; accepted 11 February 2008; published 20 March 2008.

[1] Recent reductions in both the aerial extent and thickness of sea ice have focused attention on the effect climate change is having on the polar marine system. Concomitant with a reduction in sea ice has been an increased frequency of low-pressure depressions at high latitudes. Recent studies have shown that we can expect both increased in situ cyclogenesis and advection into the arctic region. Since theses cyclones are associated with warm air advection, increased wind speed, relative humidity, and cloud cover, their impact on snow surface energy balance may be significant. The thermophysical response of snow-covered first-year sea ice to a low-pressure disturbance is investigated along with its impact on surface-based radiometer brightness temperature measurements. The data were collected during the Canadian Arctic Shelf Exchange Study (CASES) between year days 33 and 34 of 2004. Snow grain size increased throughout the sampling period with growth rates of 1.28 and 2.3 $mm^2\ d^{-1}$ for thin and thick snow covers, respectively. This rate was much faster than expected on the basis of other similar experiments documented in the literature. Furthermore, brine volume migrated upward in both snowpacks owing to the action of wind pumping affecting the dielectric constant of the snow middle layers. This increase in permittivity caused a decrease in brightness temperatures at 85 GHz of approximately 5 K and 10 K in the vertical and horizontal polarizations, respectively. This signal is sufficiently large to impact interpretation of passive microwave signatures from space.

Citation: Langlois, A., T. Fisico, D. G. Barber, and T. N. Papakyriakou (2008), Response of snow thermophysical processes to the passage of a polar low-pressure system and its impact on in situ passive microwave radiometry: A case study, *J. Geophys. Res.*, *113*, C03S04, doi:10.1029/2007JC004197.

1. Introduction

[2] Major changes have been observed in the Arctic Ocean's environment over the past 30 years [*Serreze et al.*, 2000] and sea ice depletion has been one of the most studied [e.g., *Deser et al.*, 2000; *Hilmer and Lemke*, 2000; *Wadhams and Davis*, 2000; *Rothrock and Zhang*, 2005]. Amongst other significant changes is the overall increase in occurrence and intensity of low-pressure systems through polar regions [*Zhang et al.*, 2004], and their accumulated impact on the ocean–sea ice–snow-atmosphere interface has yet to be investigated thoroughly. Studies have suggested that current temperature trends linked with climate change may allow more low-pressure systems with midlatitude origin to track northward. As these systems are generally associated with increased advection of warm air and usually strong surface flow, they have the potential to significantly alter the snow/sea ice system through enhanced forced convection. Forced convection, also termed 'wind pumping', occurs when wind disturbances create variations in surface pressure that can affect airflow within the snow [*Colbeck*, 1989]. Diffusion and convection are most likely to be enhanced by these variations, which in turn affect heat transfer and snow metamorphism [*Clarke et al.*, 1987]. Therefore, we speculate that the accumulated effects of increased cyclogenesis will have an effect on the geophysics, thermodynamics and associated radiative transfer through the snow sea ice system. These thermophysical modifications can lead to changes in microwave signatures used for snow water equivalent (SWE) estimation.

[3] The atmosphere imparts changes on the geophysics of snow covered sea ice through mass, gas and energy fluxes. Organized circulations of surface air are a result of a vertical cascade of atmospheric motion, driven by the latitudinal gradient of atmospheric density from the equator to the pole and the influence of the rotation of the earth. Extratropical and Arctic low-pressure disturbances (referred to herein as "LPDs") are of specific concern when studying cumulative effects at the surface as they result in the movement of temperature and moisture northward over a given area (classically on the eastern side of the disturbance in the Northern Hemisphere). With the advancement of a warm

[1]Centre for Earth Observation Science, Clayton H. Riddell Faculty of Environment, Earth and Resources, University of Manitoba, Winnipeg, Manitoba, Canada.

0148-0227/08/2007JC004197$09.00

boundary or 'front', increased cloudiness, temperatures and wind speeds, as well as a wind shift are observed at the surface. These characteristics have implications on sea ice growth and extent (spatial and temporal), which is controlled by the surface energy balance and snow thermophysical properties [*Maykut*, 1978; *Barber et al.*, 1994; *Perovich and Elder*, 2001; *Sturm et al.*, 2002; *Langlois et al.*, 2007a] thereby determining sea ice freezeup and melt dates [e.g., *Flato and Brown*, 1996; *Hanesiak et al.*, 1999].

[4] A pattern in regional formation zones for LPDs in the northern latitudes does exist, though frequency of cyclogenesis does vary with season [*Serreze et al.*, 2003, *Zhang et al.*, 2004]. In the context of the Canadian Arctic, the Gulf of Alaska and Baffin Bay are identified as prominent formation zones, with a greater number of disturbances originating from Alaska and extending southeastward, lee of the Rocky Mountains in Western Canada in summer. These findings correspond with the results of *Hudak and Young* [2002], where it was found that the majority of intense low-pressure system tracks originated from the "Pacific" region between the months of June to November in the Southern Beaufort Sea. In winter, the majority of disturbances are created east of Greenland, over the Barents Sea and Baffin Bay, with a noticeable maximum of LPD generation remaining in lee of the Rocky Mountains [*Serreze et al.*, 2003]. While regions of cyclogenesis in northern latitudes vary minimally from winter to summer, their intensities vary greatly [*Zhang et al.*, 2004]. Overall, LPDs that are generated in the winter are stronger than those occurring during the summer season, and those that originate from extratropical latitudes and track northward into the Arctic, particularly from oceanic origins, tend to be annually stronger than those generated locally [*Zhang et al.*, 2004]. Several LPDs were observed during the CASES overwintering study. We select one as a case study to examine the coupling between the cyclone and the geophysics/thermodynamics of the snow covered sea ice system. Polar lows last on average only a day or two. In this particular case the driver of the warm boundary was not a closed circulation in itself, but an elongated area of lower pressure extending eastward from the Gulf of Alaska to the west of the Smith Arm of Great Bear Lake. More importantly, interannual variations in frequency and intensity suggest that a larger number of more intense extratropical depressions have been migrating northward into Arctic regions over the last sixty years [e.g., *Hanesiak et al.*, 1999; *Déry and Yau*, 2002] and more of these systems are to be expected in the Arctic in a near future [*Intergovernmental Panel on Climate Change*, 2001; *Serreze et al.*, 2003; *Barber and Hanesiak*, 2004].

[5] The resulting surface energy balance variations can affect snow metamorphism, brine volume migration, thereby affecting brightness temperatures through the electrical properties of the snow cover [e.g., *Carsey*, 1992; *Armstrong et al.*, 1993; *Barber et al.*, 1995]. Many studies have examined short-term variations of spring snow covered first year sea ice [e.g., *Yackel et al.*, 2001; *Sturm et al.*, 2002] but none have assessed the effect of winter low-pressure events on the snow covered sea ice. We postulate that the remote sensing detection of the impact of low-pressure systems on the snow/sea ice system would be a useful means of monitoring the spatial and temporal periodicity of such systems in the Arctic. The accumulation of this information could also prove useful in climate modeling and process studies, which examine biogeochemical processes operating across the ocean–sea ice–atmosphere (OSA) interface.

[6] In this paper we focus on how the snow geophysical and thermodynamic processes (metamorphism, heat transfer etc) respond to a rapid change in surface pressure (and associated enthalpy) over a diurnal cycle. To the best of our knowledge this has never been done before. More specifically, the objectives of this paper are to: (1) examine snow geophysics and heat flow associated with this low-pressure disturbance and (2) to investigate the potential response of microwave radiometry to observed geophysical, thermodynamic and dielectric changes caused by the LPD. We conclude with a discussion of the implications of this case study on the broader issue of increased arctic cyclogenesis and the response of the snow/sea ice system.

2. Data and Methods

[7] Data for this paper were collected during the Canadian Arctic Shelf Exchange Study (CASES) in Franklin Bay, Northwest Territories in Canada. The Canadian Icebreaker C.C.G.S. *Amundsen* was frozen into a smooth pan of landfast first-year sea ice from December 2003 to May 2004 (Figures 1b and 1c). Although several LPDs occurred during the overwintering experiment we selected a case study of a common 'polar low' as being representative of the most common type of LPD experience during CASES. Between 2 and 3 February (day 33 and day 34) 2004, an experiment was conducted to study diurnal variations in snow thermophysical properties associated with the passage of this low-pressure system, and their effects on passive microwave brightness temperatures (T_b). We sampled geophysical properties and associated microwave brightness temperatures on a 3-hours sampling interval between 1200 local time (LT) on 2 February and 0640 am on 3 February. Air temperatures, atmospheric pressure, relative humidity and wind speed were averaged on a 10-minute interval from AXYS Automated Voluntary Observation Ship (AVOS) system mounted on the roof of the ship [*Fisico*, 2005]. An observer monitored cloud amount in octas every hour from the roof of the ship. Further details of this sampling period are available elsewhere [*Langlois et al.*, 2007a, 2007b].

2.1. Geophysical and Electrical Data

[8] A total of 14 thin and thick snow pits (7 thin/thick snowpit combinations) were sampled within 30 minutes time interval with the surface based radiometer (SBR) measurements (Table 1). The snowpits were separated in 2-cm layers for both thin and thick snow. Thin snow was measured at 6 cm and thick at 16 cm. The layer L2_si represents the bottom 2 cm in contact with the ice surface whereas layers L6_4 and L16_14 represent the top layer for both thin and thick snow respectively. Vertical snow temperature profiles at a 2-cm resolution were measured using a Hart Scientific temperature probe. The temperature was measured immediately after the snow pit was excavated to avoid bias with air contact. Snow wetness was derived from conductivity measurements using a capacitance plate, which measures the increased conductivity of snow with the addition of liquid water. Snow grain sizes were measured in the ship's cold laboratory, which was maintained at

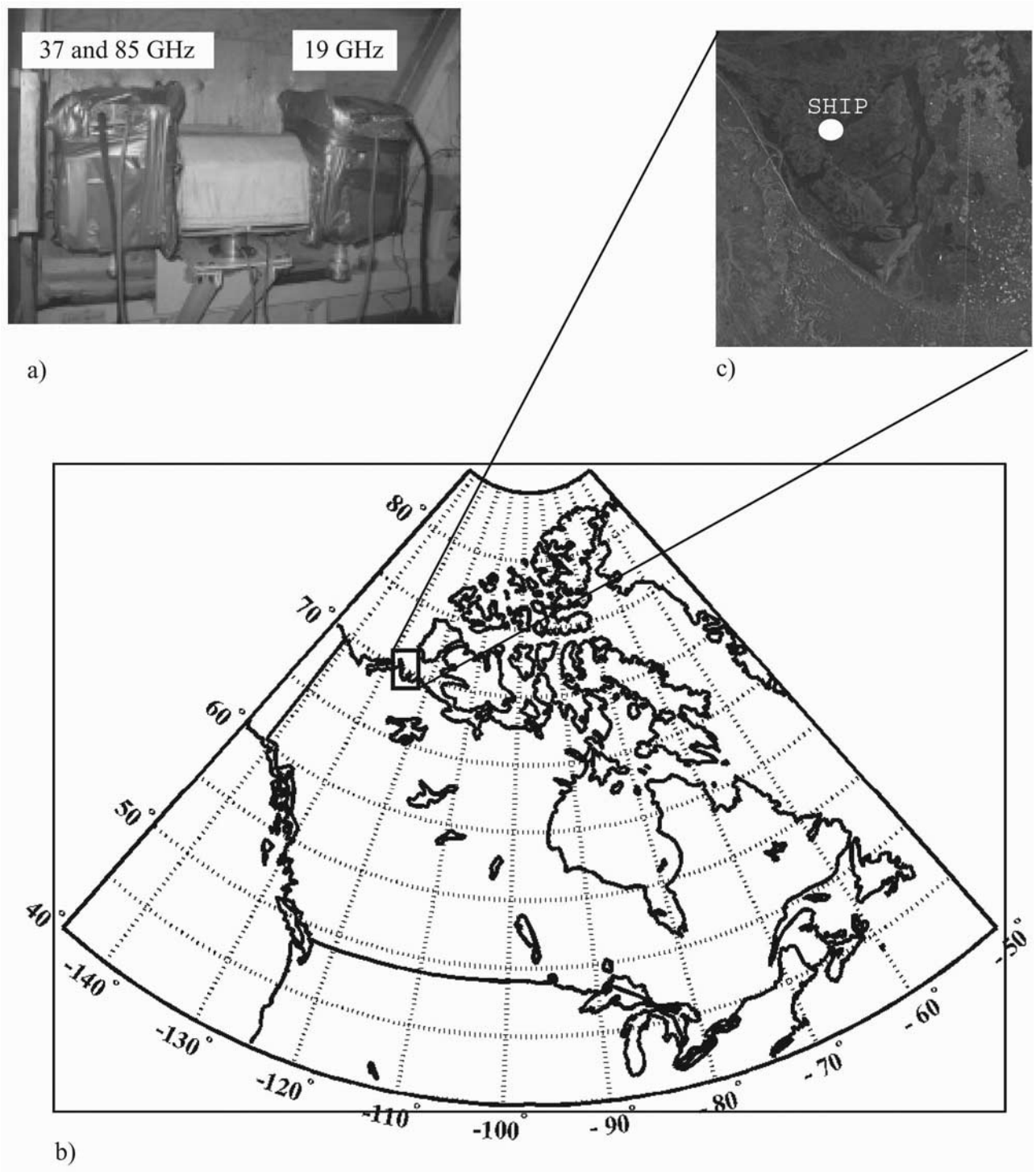

Figure 1. (a) SBR setup on the C.C.G.S. *Amundsen*, with (b) a map of the study location and (c) a RADARSAT image close-up on the ship's overwintering position in Franklin Bay.

temperature of −20°C throughout our experiment. Pictures of snow grains were taken using a digital camera (Canon Powershot 5 megapixels) mounted on a stereomicroscope (Leica M7.5). The pictures were then digitized using a purpose built polygon analysis Matlab program to extract median and average grain sizes.

[9] As temperature gradient and vapor pressure are essential to understand snow metamorphism [e.g., *Colbeck*, 1993; *Langlois et al.*, 2007a] we considered the saturation vapor pressure of ice (e_{si}) as

$$e_s(T) = \mathrm{A} \cdot e^{-B/T}, \tag{1}$$

where A and B are pressure and temperature constants according to ice, and T is the volume temperature in Kelvin [*Rogers and Yau*, 1989]. The only variable used in this

Table 1. Sampling Times for Thin/Thick Snow Covers and Surface-Based Radiometer Measurements[a]

	Snow		
Flag	Thick	Thin	SBR
SP1	1208	1250	1151
SP2	1500	1525	1435
SP3	1800	1830	1735
SP4	2100	2130	2143
SP5	0005	0035	2333
SP6	0300	0330	0243
SP7	0605	0640	0538

[a]Times are given as local ship time.

calculation of vapor pressure was the snow physical temperature. The effect of salinity/brine volume is considered such as

$$e_s(T) = e_s(T) \cdot (1 - 0.000537 \cdot S), \tag{2}$$

where e_s (T) is the vapor pressure in function of temperature from equation (1) and S the salinity in ppt of the considered volume. Snow density was measured using samples from density cutters (66.36 cm^3), which were weighted in the cold room shortly after the snowpit was dug. Salinity was measured using melted snow samples using a conductivity meter (Hoskin Scientific WTW 330i). The brine volume fraction in snow is found by [*Drinkwater and Crocker*, 1988]

$$V_b = \left[\frac{v_b \rho_b}{(1 - v_b)\rho_i + v_b \rho_b}\right]\left[\frac{\rho_s}{\rho_b}\right], \tag{3}$$

where ρ_s is the density of the snow sample in g cm^{-3}, ρ_i is the temperature-dependent density of pure ice. T_s is the temperature of the snow sample in °C, and the density of brine ρ_b in g cm^{-3} is a function of the brine salinity [*Cox and Weeks*, 1982]. The salinity of brine S_b is also a function of temperature following *Assur* [1958] and *Poe et al.* [1972]. The brine volume v_b of ice/brine mixtures at a given temperature is obtained following *Assur* [1958], *Frankenstein and Garner* [1967], and *Poe et al.* [1972].

[10] Both permittivity and dielectric loss of snow over first-year sea ice can be calculated from a dielectric mixture model [*Barber and Thomas*, 1998; *Barber et al.*, 2003] of the form proposed by Polder-Van Santen and later modified by de Loor [*Ulaby et al.*, 1986] using snow wetness, temperatures and salinity measurements. Although the results are not shown here, the dielectric constant over sea ice can be computed for 19 and 37 GHz. Since the Polder-Van-Santen approach assumes the absorption to be the main extinction mechanism, the upper limit (frequency) for the application of the model is unknown. Therefore, the dielectric constant provided here are for 37 GHz. Obviously, the values at 19 or 85 would be different, but we were interested in the timing and direction of the changes and the computation at 37 GHz are suited for our interpretation.

[11] Measurements of snow permittivity and wetness on sea ice rely on capacitance probes [*Denoth*, 1994; *Barber et al.*, 1995]. However, in the presence of brine, a permittivity-brine wetness relationship is needed to estimate brine volume [*Barber et al.*, 1995; *Drobot and Barber*, 1998; *Langlois et al.*, 2007a]. This technique uses a capacitance plate, which measures the increased conductivity due to small amounts of water in liquid phase [*Denoth*, 1989]. The effective measuring area of the capacitance plate is 12.5 × 13 cm at an operating frequency of 20 MHz. The permittivity ε is given by

$$\varepsilon = 1 + k \cdot \log_{10}\left(\frac{U}{U_{ref}}\right), \tag{4}$$

where k is the sensor specific calibration constant, U and U_{ref} are the readings within the snow and in air respectively. The readings display numbers related to the actual capacity of the dielectric sensor. With density measurements and permittivity values from the equation above, liquid water content can be derived as shown in

$$\varepsilon = 1 + 1.92\rho + 0.44\rho^2 + 0.187W_v + 0.0046W_v^2. \tag{5}$$

[12] This technique has an estimated precision of 0.5 of one percent water by volume when there is no brine in the snow layer. The technique is unable to measure W_v in the highly brine saturated basal layer of snow on first-year sea ice forms owing to the elevated dielectric constant of this volume and the lack of suitable calibration. Further details are available elsewhere [*Barber et al.*, 1995]. Wetness below 1% is considered 'dry' and treats brine as "inclusion dielectric" within a dry snow "host dielectric" [*Barber et al.*, 1995] (after *Matzler* [1987] and *Drinkwater and Crocker* [1988]). The 1% represents the wetness values where water becomes free within the snowpack [*Barber and LeDrew*, 1994]. This is where the dielectric properties change considerably. The relationship has been determined empirically [*Tiuri et al.*, 1984]. Further details on the dielectric modeling is given by *Langlois et al.* [2007b].

2.2. Thermodynamic Processes

[13] In order to understand thermodynamic processes such as metamorphism occurring within the snow under the passage of a LPD, snow thermal conductivity and diffusivity were calculated. Snow thermal conductivity (k_s) calculations were made following *Ebert and Curry* [1993] accounting for both temperature and density,

$$k_s = 2.845 \cdot 10^{-6} \cdot \rho^2 + 2.7 \cdot 10^{-4} \cdot 2^{\frac{(Ts-233)}{5}}, \tag{6}$$

where ρ is snow density (kg m^{-3}) and T the temperature (K). Snow thermal diffusivity (v_s) was calculated following *Oke* [1987],

$$v_s = \frac{k_s}{\rho_s \cdot c_s}, \tag{7}$$

where ρ_s and c_s represent the density of snow (kg m^{-3}) and the specific heat (J kg^{-1} K^{-1}) where the heat capacity (C_s, J m^{-3} K^{-1}) is the product between ρ_s and c_s. From these thermal parameters, we retrieved vapor flux values following *Colbeck* [1993],

$$J = -D \cdot \frac{\partial \rho}{\partial z}, \tag{8}$$

where J is the vapor flux (kg m^{-2} s^{-1}), D the diffusivity of water vapor (mm^2 s^{-1}) in air and $\partial\rho/\partial z$ the vapor density gradient. For saturated conditions, the vapor flux can be expressed in terms of temperatures and temperature gradient after *Sturm and Benson* [1997] and *Baunach et al.* [2001],

$$j\left(T, \frac{\partial T}{\partial z}\right) = -\frac{D}{R}\frac{p_v(T)}{T^2}\left[\frac{L}{RT} - 1\right]\frac{\partial T}{\partial z}, \quad (9)$$

where D is p_v is the saturation vapor pressure for ice, L is the latent heat of sublimation (2838 J g^{-1}) and R is the gas constant for water vapor (0.4619 J g^{-1} °C^{-1}). Under temperature gradient metamorphism, grain growth increases the fractional volume of air (decrease in number density), which low thermal conductivity and diffusivity increase the temperature gradient accelerating the initial grain growth [e.g., *Izumi and Huzioka*, 1975; *Colbeck*, 1997; *Sturm and Benson*, 1997]. Previous studies looking at physical values of vapor fluxes from one layer to another were successful over land [*Trabant and Benson*, 1972; *Sturm and Benson*, 1997], but further study is required for snow on sea ice.

2.3. Brightness Temperatures

[14] The SBR (Figure 1a) was located at a height of 13 m above the surface. Measurement cycles consisted of a 3-minute exposure time where the SBR measured brightness temperatures (T_b) every 5 seconds at an incidence angle of 53°. Multiple incidence angles were also used between 30° and 70° with an elevation increment of 5°. The ship was in a fixed location throughout the study period where snow was initially naturally distributed in the ship's surrounding. As the season progressed, snowdrifts were created so that thin snowpacks were found in the proximity of the ship (<15 m) while thicker snow was found farther from the ship (>15 m). Therefore, the SBR low incidence angles (30° to 45°) measured emissions from thin snow (6 cm) and larger incidence angles (55° to 70°) measured emission from thicker snow (16 cm). Absolute calibration for the measured brightness temperatures were done following *Grenfell and Lohanick* [1985] and *Asmus and Grant* [1999].

3. Results

[15] From October 2003 to June 2004, a total of 42 LPDs were documented in the Canadian Arctic Shelf Exchange Study (CASES) region (Figure 1), with 55% of those originating from the Arctic, 40% originating from the Pacific, and 5% of the total originated from irregular sources where the most synoptically active months were November and March. Early season disturbances developed and terminated west of the ship location providing the Southern Beaufort Sea with warm and moist air from southern latitudes. This coincides with previous findings in our climatological investigation, where it was found, especially during the months of October and November, that temperature and moisture over the Beaufort Sea were anomalously positive compared to previous years. Conversely, in the late winter/early spring months, very little cyclonic activity was noted, indicating a strong and persistent Arctic High for much of the period, allowing the advection of frigid arctic air into the CASES region for much of this time and causing lower than normal temperatures and moisture content. It is apparent that low-pressure systems affect the southern Beaufort Sea throughout the annual cycle. The role of these pressure systems on the seasonal/annual forcing of the ocean-ice-atmosphere system is the topic of other work arising from our lab and beyond the scope of this particular paper. In what follows we focus only on the atmosphere-surface coupling associated with our case study.

3.1. Micrometeorological Data

[16] The atmospheric pressure on day 32 was, on average, 1020 mbar until the low-pressure system decreased the values slowly to an average of 1014 mbar on the morning of day 34 (between 0400 and 1200 LT on Figure 2a). A slight increase was measured between the two first sets of snowpits (SP1 and SP2) at 1300 LT (Figure 2b), but the most significant warming occurred overnight between SP4 and SP7 where the maximum temperature reached −23.8°C shortly before 0400 LT on day 34. The increase rate was on the order of +0.6 °C h^{-1} between 1600 LT and 0400 LT. Relative humidity increased slightly over the diurnal period (Figure 2c) and wind speed (maximum recorded at 0400 LT on day 34 on Figure 2d). A shift in wind direction was also measured at the end of the depression where the direction varied from below 100° at 1900 LT on day 33 to over 300° at 2200 LT on the next day (Figure 2e). The total cloud cover increased from 0 to 8 octas over day 33 and remained mostly covered until day 35 (Figure 2f).

3.2. Thin Snow Cover

3.2.1. Physical and Electrical Data

[17] Snow volume temperatures in thin snow increased significantly throughout day 33 (Figure 3a). Values started at a minimum of −28°C and −24.4°C for both layer 6_4 (L6_4) and layer 2-si (L2_si) respectively at 1250 LT, and maximum temperatures were reached at 0035 LT (warming rate on the order of +0.47°C h^{-1} for L6_4 and +0.43°C h^{-1} for L2_si). The temperature gradient reached 1.2 °C cm^{-1} compared to 0.65 °C cm^{-1} on the last series of snowpits (SP7 on Figure 2a) on day 34. Snow density was practically unchanged where small variations are due to the uncertainty with the sampling methodology and natural small-scale variability. On average, density at the top of the snowpack was 270 kg m^{-3} and 240 kg m^{-3} at the bottom. Salinity at both L4_2 and L6_4 increased between day 34 and day 35 where values peaked from 8.3 to 18 ppt and 1.8 to 5.6 ppt for L4_2 and L6_4, respectively. Values at L2_si remained high between 20 and 25 ppt without following any particular trend (Figure 4a). Concordantly, brine volume increased for both L6_4 and L4_2 and reached a maximum at 0300 LT where the values doubled. The most significant increase was measured at L4_2 with an increase of 153% between 1250 LT on day 33 and 0330 LT on day 34. Values at the bottom L2_si varied between 1.2% and 1.9% with a minimum measured at 1525 LT and a maximum at 1830 LT on day 33 (Figure 4b).

[18] Thin snow permittivity values remained relatively stable for L6_4 and L4_2 averaging 1.52 and 1.54 until 2130 LT (Figure 5a). The lowest value of 1.41 was recorded at 1525 LT at L2_si, then increased until 2130 LT where all layers had similar values at 1.55, 1.51 and 1.50 at L6_4, L4_2 and L2_si, respectively. A sharp increase was mea-

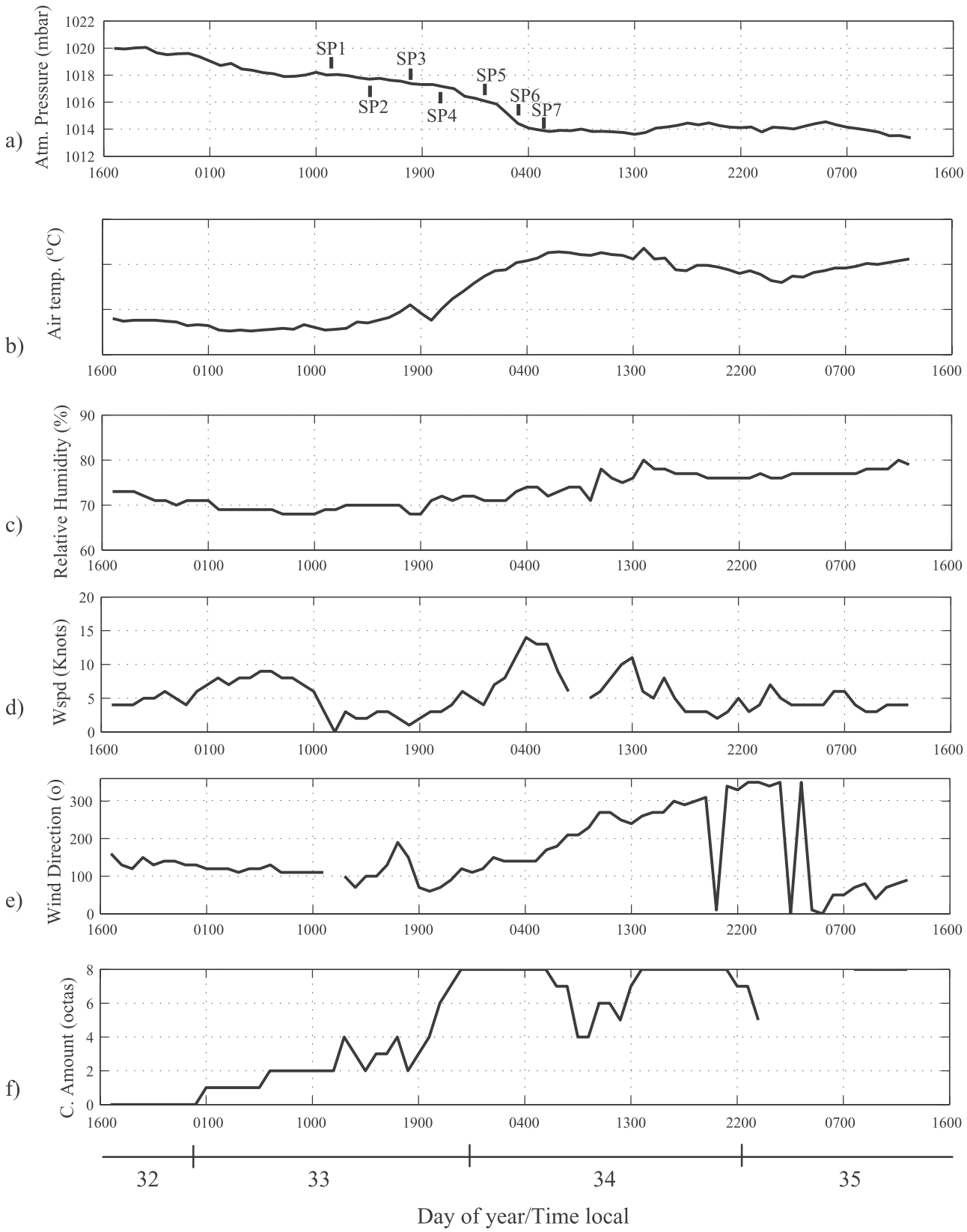

Figure 2. Temporal evolution of (a) atmospheric pressure, (b) air temperature, (c) relative humidity, (d) wind speed, (e) wind direction, and (f) cloud fraction.

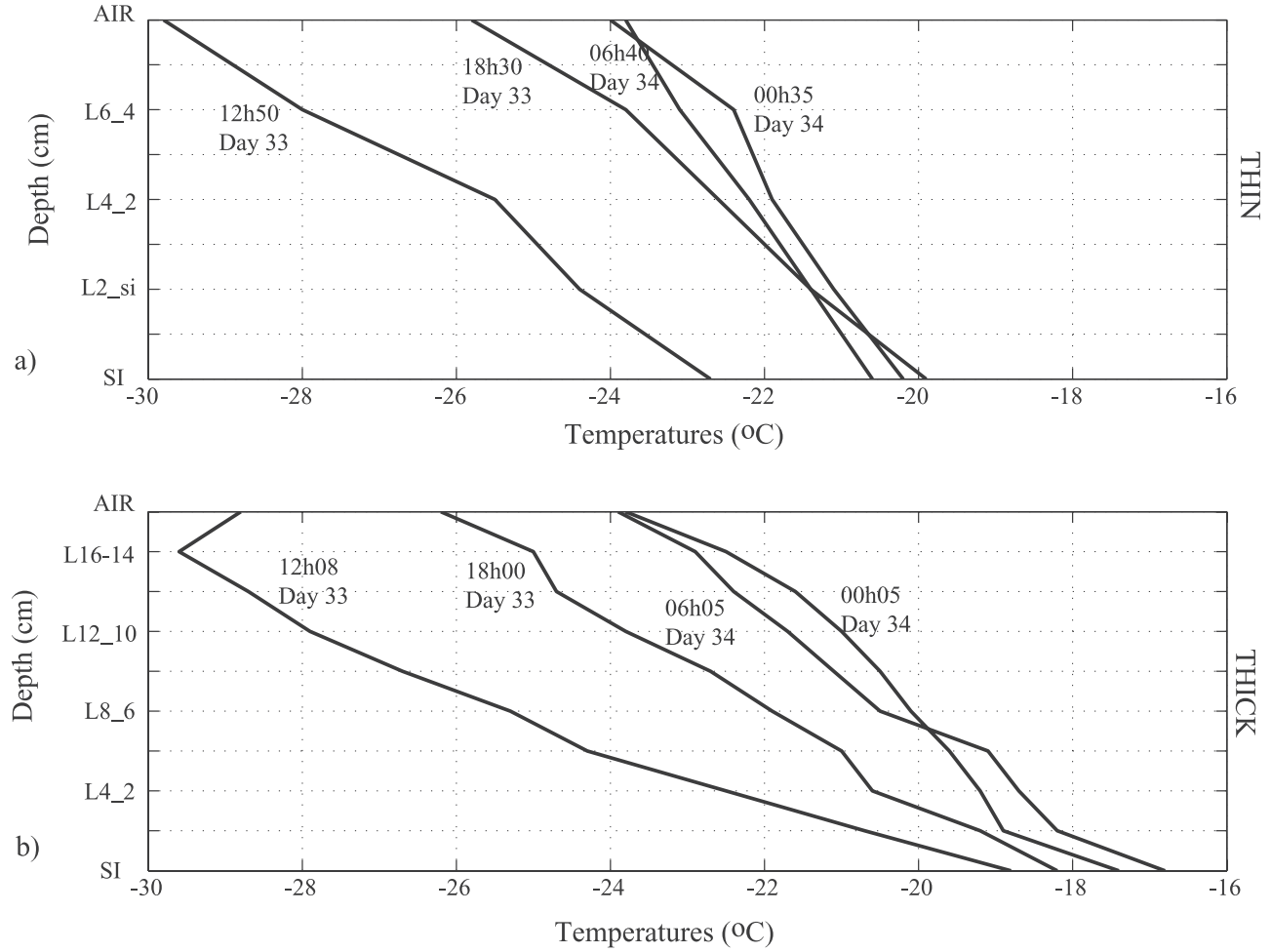

Figure 3. Temporal evolution of (a) thin snow temperature gradient and (b) thick snow temperature gradient.

sured at L4_2 until the end of the sampling period where values jumped from the average of 1.54 prior to 2130 LT up to 1.81 at 0640 LT on day 34. Values at L6_4 and L2_si were similar to each other within 0.01. The dielectric loss was very low at L6_4 as it increased by a factor of 10 at L4_2 from 0.004 at 1250 LT on day 33 to a maximum of 0.044 at 0330 LT on day 34 (Figure 5b). The values at L2_si remained relatively stable oscillating slightly around an average of 0.051.

3.2.2. Heat/Mass Transfer and Snow Metamorphism

3.2.2.1. Thermal Conductivity and Diffusivity

[19] The thermal conductivity of both bottom and top layers did not vary significantly throughout the sampling period (Figure 6a). Large variations were measured at L4_2 where k_s decreased until 2130 LT (0.095 W m^{-1} K^{-1}) and then increased significantly until the end of the sampling period, reaching a maximum of 0.258 W m^{-1} K^{-1}. Specific heat values remained unchanged in the top layer (Figure 6b). However, an increased was measured between 1830 and 0035 LT for both L4_2 and L2_si where values reached a maximum of 2428 and 2928 J kg^{-1} K^{-1}. The values then decreased significantly to 2059 and 2021 J kg^{-1} K^{-1}, three hours later. Values of thermal diffusivity were proportional to k_s for both L6_4 and L2_si with minimum values of 1.56 and 1.12 $\times$ 10^{-7} m^2 s^{-1}, respectively at 0035 LT (Figure 6c). Thermal diffusivity values at the middle layer increased after 2130 LT from 1.5 to 2.96 $\times$ 10^{-7} m^2 s^{-1} at 0640 LT on day 34.

3.2.2.2. Vapor Flux and Snow Metamorphism

[20] The average vapor flux was +1.5 $\times$ 10^{-7} kg m^{-2} s^{-1} ($\pm$0.78 $\times$ 10^{-7}) with positive values (gain in mass) throughout the sampling period. Accordingly, snow grain size increased approximately 1 mm^2 (Figure 7) when values where at maximum measured at 0640 LT on day 34 (5.69 mm^2). The growth rate was approximately 0.053 mm^2 h^{-1} over the 18-hour period, suggesting a daily increase of 1.28 mm^2 d^{-1} when applying a least squares linear relationship to the data. The increase in grain size was coincident with increased saturation vapor pressure at the basal layer of 0.023 kPa throughout the sampling period with an R^2 of 0.58.

3.2.3. Brightness Temperatures

[21] The minimum brightness temperatures values over thin snow were reached at 1435 LT after which a significant increase of approximately 0.3 K h^{-1} was measured until 2333 LT for both 19 and 37 GHz (Figures 8a, 8b, 8c, and 8d). The vertical polarization (V-pol) values were higher throughout the sampling period and the difference between

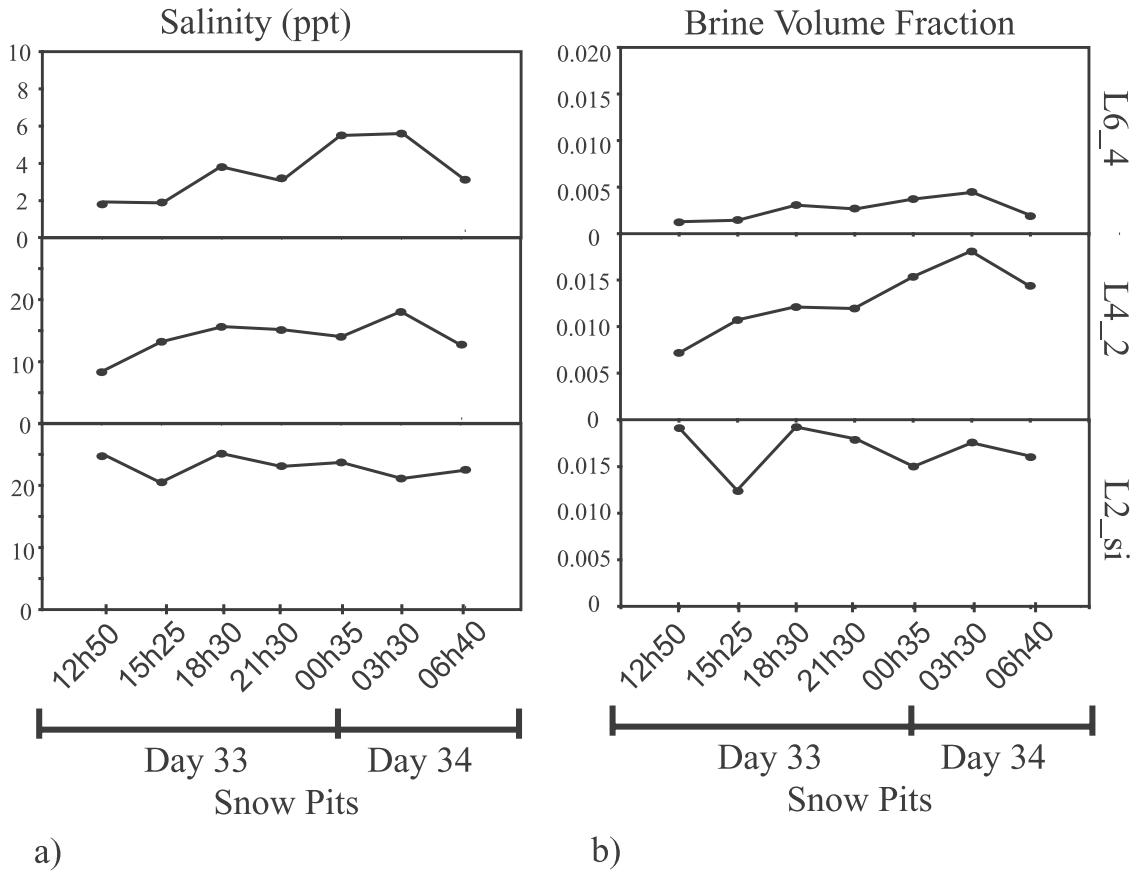

Figure 4. Temporal evolution of (a) salinity and (b) brine volume fraction for thin snow.

19 and 37 GHz (ΔT_b) was very small. Brightness temperatures at 85 GHz warmed up quicker than 19 and 37 GHz until the maximum was reached at 2333 LT (Figures 8e and 8f). A significant decrease, on the order of 4 K in V-pol (Figure 8e) and 8 K in H-pol (Figure 8f), was measured at 0243 LT for all incidence angles and both polarizations.

3.3. Thick Snow Cover

3.3.1. Physical and Electrical Data

[22] Thick snow volume temperatures increased throughout the vertical profile (Figure 3b) and a warming rate was higher near the snow cover surface where values increase by 0.5 °C h^1 at L16_14 compared to 0.2 °C h^1 at L2_si. The difference between the top and the bottom of the snowpack was then 10 °C, which corresponded to a gradient of 0.63 °C cm^{-1} compared to 0.44 °C· cm^{-1} at the end of the sampling period on day 34 (Figure 3b). Averaged snow density values remained high throughout the snowpack with the exception of L2_si. The average value for L2_si is 233.96 kg m^{-3} as it varied between 302.56 and 393.17 kg m^{-3} for the remainder of the vertical profile. Maximum salinity values were reached at 0300 LT for all layers between L6_4 and L16_14 (Figure 9a). Values at the bottom layers L4_2 and L2_si remained high throughout the diurnal study with averages of 8.7 and 19.8, respectively. Brine volume at L2_si decreased slightly until 1800 LT on day 33 as the decrease was measured until 2100 LT at L4_2 (Figure 9b). Afterward, values increased until the end of the sampling period for L2_si (69% increase) whereas L4_2 was variable with a maximum value reached at 0005 LT.

[23] The permittivity values in thick snowpacks did not follow any significant trends throughout the diurnal period (Figure 5c). However, two distinct peaks are measured at 1500 LT and 0300 LT at the surface layer L16_14 where the values reached 1.79 and 1.72, respectively. The two peaks were measured at L16_14 (i.e., surface layer) where the salinity is negligible. Hence, the two peaks observed are probably due to variations in snow density, however, this variation is most likely due to sampling errors. The permittivity at L10_8 and L2_si were relatively unchanged between 1208 LT on day 33 and 0005 LT on day 34 with a very small peak at 2100 LT at both layers. A significant decrease was measured at L10_8 and L6_4 between 0005 LT and 0300 LT where the minimum values were reached at 1.51 and 1.52, respectively. The dielectric loss was quite stable for the top two layers at a small average of 0.005 (Figure 5d). Values at L6_4 peaked at 1500 LT on day 33 to a dielectric loss close to 0.02. A visible plateau is observed between 2100 LT and 0300 LT on day 34 at around 0.02, then decreased back to values close to 0 at the end of the sampling period. The strongest variations were measured at L2_si with a maximum value of 0.078 at 1800 LT and a minimum of 0.037 recorded at 0300 LT.

3.3.2. Heat/Mass Transfer and Snow Metamorphism

3.3.2.1. Thermal Conductivity and Diffusivity

[24] The thermal conductivity decreased in the layers L10_8 and L6_4 until 0300 LT on day 34 whereas values

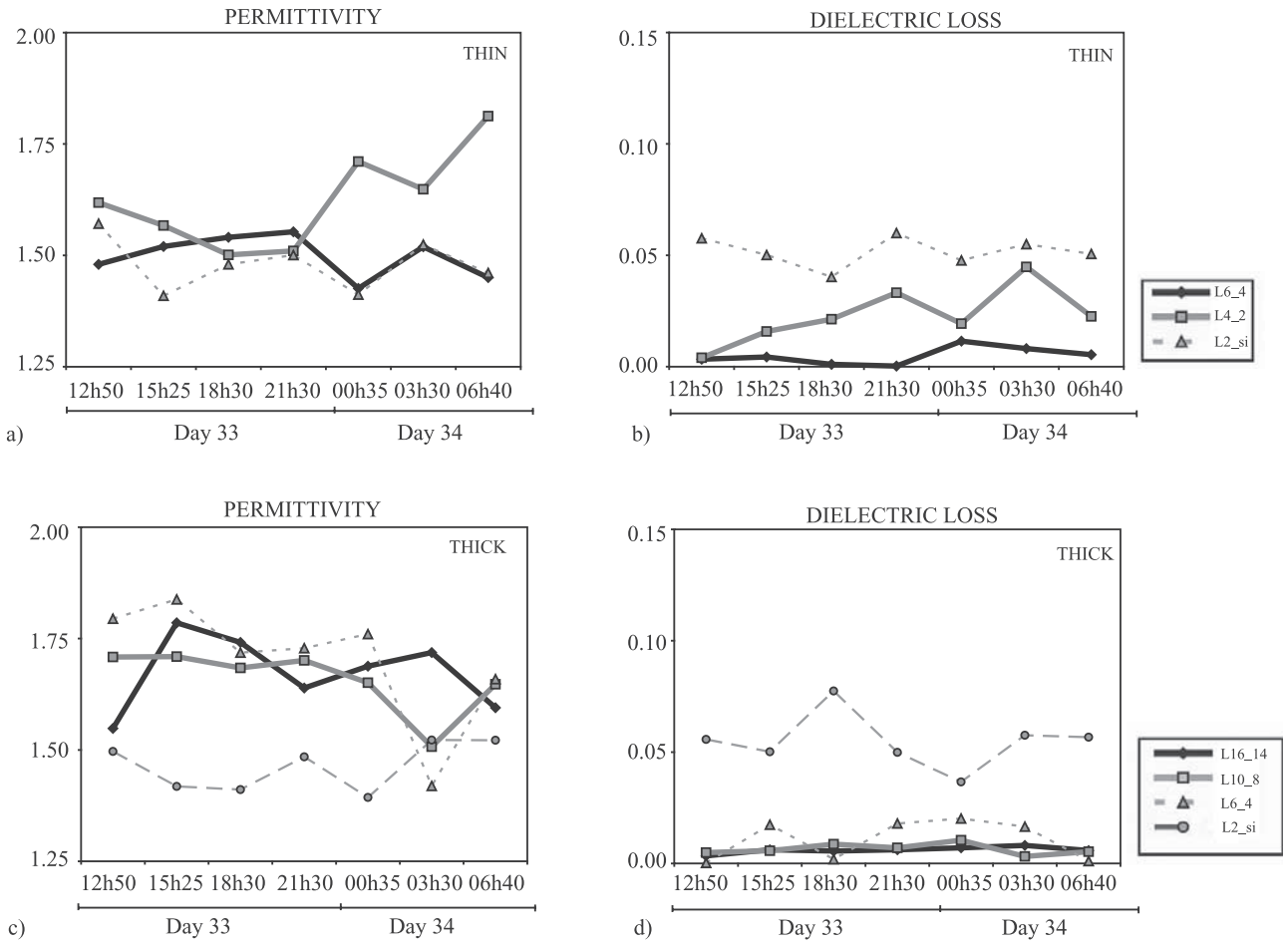

Figure 5. Temporal evolution of thin snow (a) permittivity and (b) dielectric loss, and thick snow (c) permittivity and (d) dielectric loss.

remained stable throughout the period for L2_si (Figure 10a). The decrease was significant between 0035 and 0300 LT where the minimum was reached at 0.1 and 0.07 W m^{-1} K^{-1} for both L_10_8 and L6_4, respectively. Surface k_s values were variable between 0.13 and 0.27 W m^{-1} K^{-1} without following any apparent trend. Values of specific heat (Figure 10b) were stable for the near-surface layers as an increase was measured between 1500 and 1800 LT at L2_si (from 2150 to 2368 J kg^{-1} K^{-1}). Specific heat at layer L6_4 remained unchanged until 0300 LT where a peak was measured increasing c_s of over 500 J kg^{-1} K^{-1} to reach a maximum value for the sampling period at 2604 J kg^{-1} K^{-1}. The peak was also measured at L4_2 and with smaller amplitude at L8_6 (not shown on Figure 10b). The thermal diffusivity followed the same trends as measured for k_s with a decrease at the middle layers and stable L2_si (Figure 10c). We again measured a significant decrease at 0300 LT for L10_8 and L6_4 where the values reached the minimum for the sampling period at 1.74 and 1.26 m^2 s^{-1}, respectively.

3.3.2.2. Vapor Flux and Snow Metamorphism

[25] The average vapor flux was $+1.93 \times 10^{-7}$ kg m^{-2} s^{-1} ($\pm 0.71 \times 10^{-7}$) again with positive values (gain in mass) throughout the sampling period. The total snow grain growth was measured at approximately 1.8 mm^2 and the maximum was reached at 0300 LT (6.5 mm^2). The growth rate was 0.096 mm^2 h^{-1} corresponding to a daily growth of 2.3 mm^2 d^{-1}. The saturation vapor pressure also increased accordingly at L2-si from 0.095 to 0.126 kPa at 0300 LT where the maximum grain size was reached. Both grain size and saturation vapor pressure were directly proportional with a R^2 value of 0.72.

3.3.3. Brightness Temperatures

[26] Overall, the brightness temperatures at both 19 and 37 GHz increased throughout the diurnal study (Figures 8a, 8b, 8c and 8d) for thick snow incidence angles (53° and 70°). The maximum values were reached at 2333 LT for all frequency/polarization/incidence angle combinations with a warming rate of 0.34 and 0.4 K h^{-1} for 53° and 70°, respectively. In the vertical polarization, T_b's were higher at an incidence angle of 53° as they are at 30° in the horizontal polarization. As we observed in thin snow covers, 85 GHz brightness temperatures decreased at 0243 LT in both polarizations (Figures 8e and 8f). The decrease was on the same order of magnitude as measured over thin snow (i.e., 4 K in the V-pol. and 8 K in the H-pol.).

4. Discussion

4.1. LPD and Observed Changes in Snow

[27] The passage of a low-pressure system produced detectable changes in snow geophysical properties including temperature and brine volume. As mentioned in the

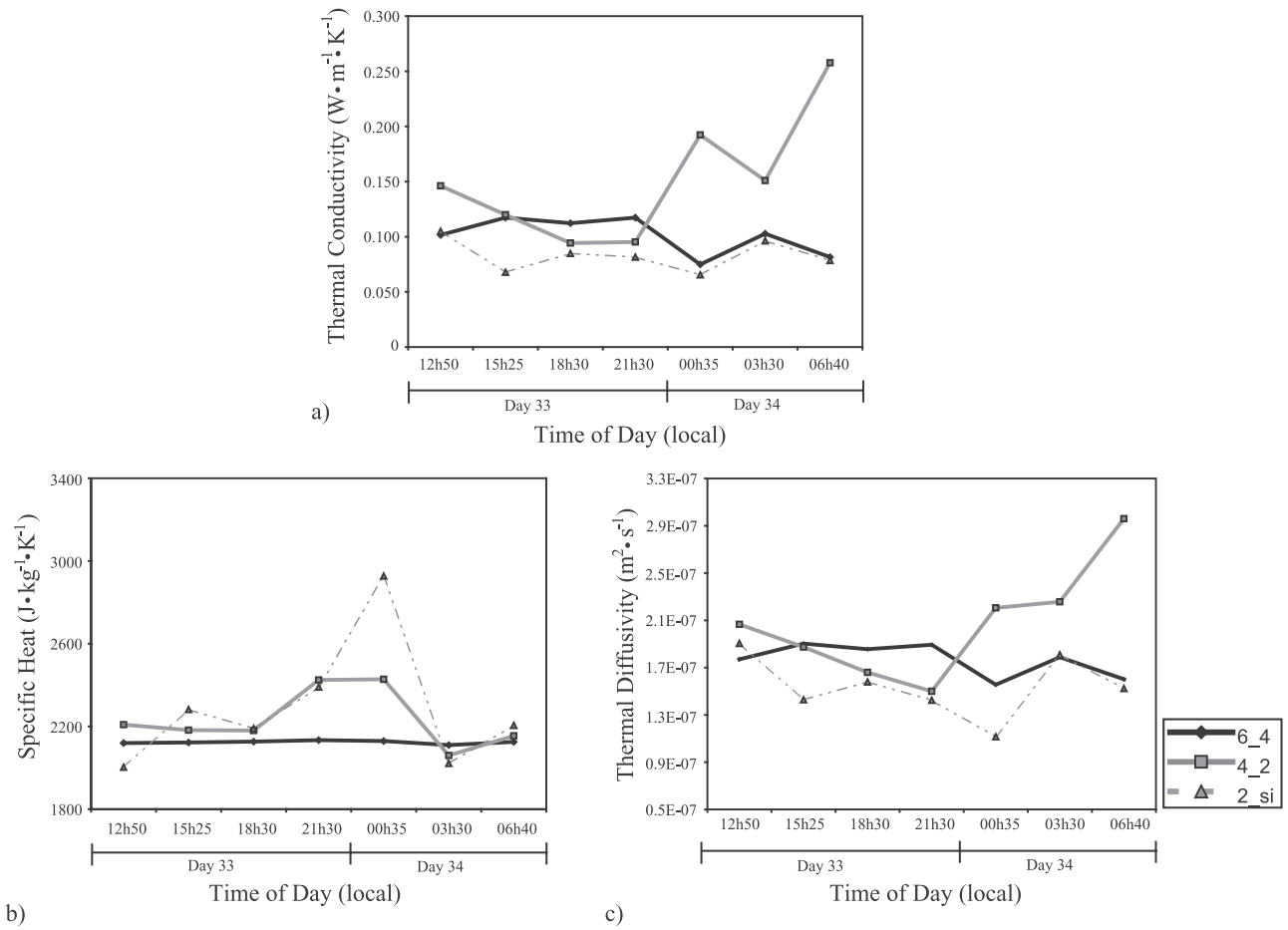

Figure 6. Temporal evolution of (a) thermal conductivity, (b) specific heat, and (c) thermal diffusivity for thin snow.

introduction, LPDs are associated with a decrease in surface pressure and an increase in temperatures, cloudiness and wind speed. Those changes occur within hours and affect snow geophysical properties and brightness temperatures. Such surface disturbance leads to wind pumping, known to change heat and mass transfer as highlighted in section 3. The increased convective transfer leads to grain growth [e.g., *Sturm and Benson*, 1997], which rate is faster than stable conditions. These conditions will favor upward brine migration which results in an increase dielectric constant. We speculate that the amplitude of the change and detectability is proportional to the strength of the disturbance. The details of the resulting changes are discussed below for thin (section 4.2), thick snow (section 4.3) along with the concordant changes in brightness temperatures (section 4.4).

4.2. Thin Snow Processes

[28] The increase in salinity comes from the brine migration in the upper layer of the snowpack through convective processes. The convection is associated with the passage of the LPD that allows brine to move from very saline layers toward the bottom of the snowpack to middle layers, which causes salinity values to increase. Brine volume migrated upward within the air pores in L4-2 as depicted in Figure 4b. Concordantly, k_s increased significantly between 2130 and 0640 LT since brine volume thermal conductivity is close to ice ($\sim$1.6 and 2.2 W m^{-1} K^{-1}), which is much higher than k_{air} at $\sim$0.025 W m^{-1} K^{-1} [*McKay*, 2000; *Pollard and Kasting*, 2005]. Furthermore, the migration of brine within a layer increased the specific heat until 0035 LT [*Pollack et al.*, 2003]. Such increase is translated by a decrease in thermal diffusivity as more energy is used within one layer (i.e., less available for diffusion). We observed this inversely proportional relationship on Figures 6b and 6c as the maximum c_s values at 0035 LT correspond to the minimum value of v_s [*Yen*, 1981; *Sturm et al.*, 1997]. This concept is of primary importance owing to its control on the snow/ice interface temperatures [*Sturm et al.*, 1997; *Bartlett et al.*, 2004], which in turn can greatly affect microwave emission and scattering mechanisms [*Eppler*, 1992]. This concept will be discussed in details in the following section.

[29] We showed over the diurnal period that there was a detectable increase in grain size under a LPD. *Langlois et al.* [2007a] measured growth rate of 0.25 mm^2 d^{-1} in thin snow covers (4–10 cm) during the coldest season, a much lower value that what was measured in this study (1.28 mm^2 d^{-1}). The temperature gradient (Figure 7) we measured in this study (maximum of 1.2 °C cm^{-1} at 1250 LT) is sufficient to induce snow grain metamorphism, which seemed to occur throughout our sampling period [e.g., *Bergen*, 1968; *Colbeck*, 1982, 1993]. Interestingly, *Colbeck* [1980] showed that a local temperature gradient as small as

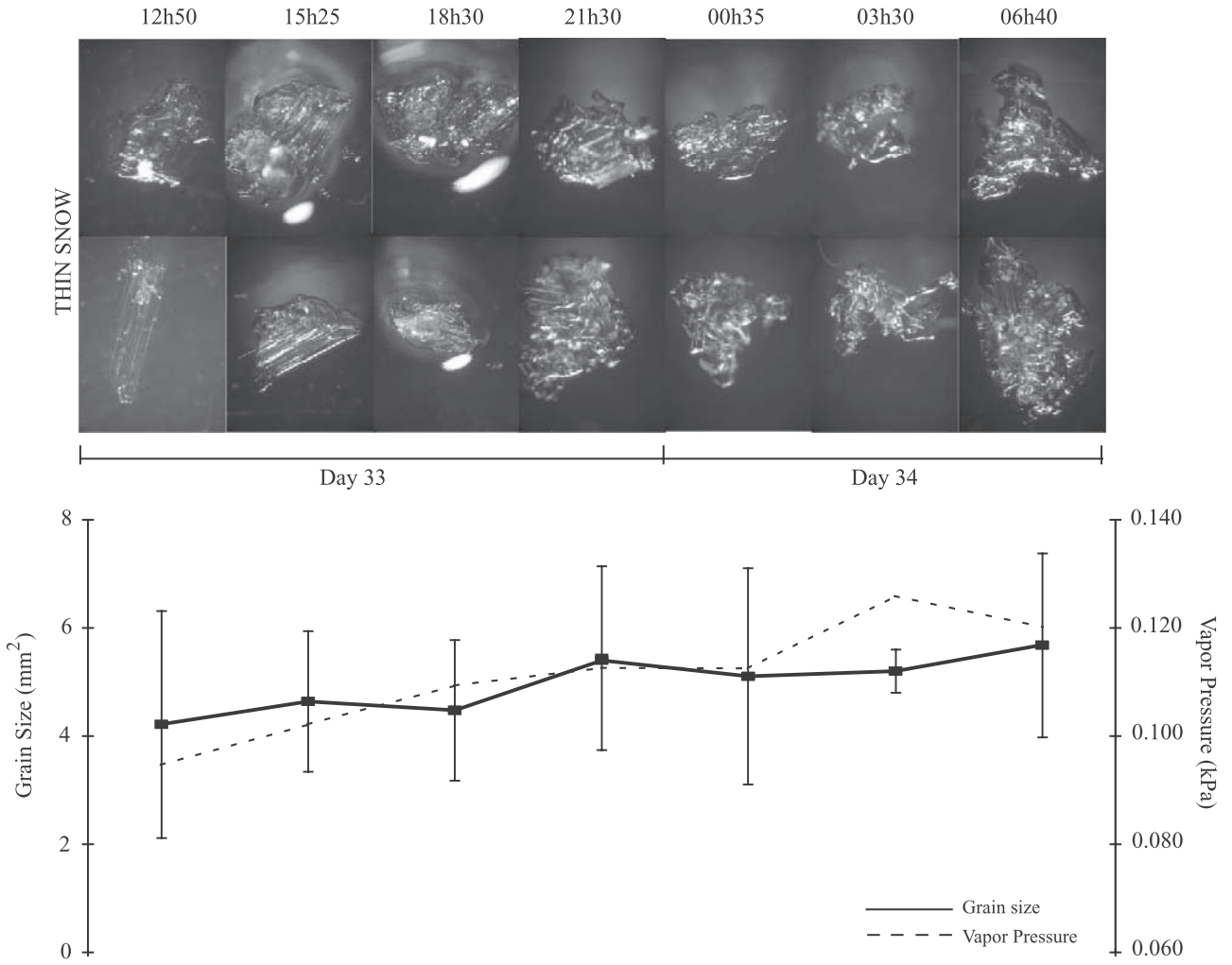

Figure 7. Temporal evolution of thin snow grain size and saturation vapor pressure.

10^{-2} °C cm^{-1} could result in a grain growth of 0.1 mm. We speculate from this results that grain growth may be episodically large under the influence of LPDs and that the accumulation of many LPD events may have a cumulative effect on the mid pack snow grains, and through this on the surface albedo.

[30] The vapor flux was on average $+1.5 \times 10^{-7}$ kg m^{-2} s^{-1}, which positive value suggests a gain in mass [*Sturm and Benson*, 1997], but no other data set provides such data over first-year sea ice. However, work done by *Sokratov and Maeno* [2000] suggests that our vapor flux values fall within the range of what they measured over land. Since the diurnal period occurred in the cooling period [see *Langlois et al.*, 2007a], we looked at the vapor flux values under high-pressure systems to see if any differences exist between the two cases. Between day 57 and 62, a high-pressure system was located over the region and concordant snowpit analysis showed vapor fluxes of -1.22×10^{-7} kg m^{-2} s^{-1} suggest a loss of mass due to sublimation [*Sturm and Benson*, 1997; *Baunach et al.*, 2001]. We also calculated the vapor flux between days 37 and 41 where another important high-pressure system resulted in vapor flux values oscillating around 8×10^{-7} kg m^{-2} s^{-1}. Since both systems resulted in lower vapor pressure values than under a LPD, we can speculate that the vapor flux is accelerated by low-pressure systems. We note that further investigations are required to further refine this speculation. However, the temperature gradient between day 37 and 41 were lower (average of 1.22 and 0.98 °C cm^{-1} through L6_4 and L2_si, respectively) than recorded on the previous snow sampling set on day 31 (average of 2.35 and 2.1 °C cm^{-1}). Assuming an accelerated vapor flux, snow grain kinetic growth is expected to increase [*Albert*, 2002].

4.3. Thick Snow Processes

[31] The upward brine migration measured in thin snow covers was also measured in thick snow as shown in Figure 9b. There is no evidence of increasing permittivity and dielectric loss (Figures 5c and 5d) in the middle layers due to discrepancies in the density measurements affecting the dielectric calculations. The variations measured in the density values were too large to be natural thereby significantly affecting the dielectric calculations. The decrease at L10_8 and L6_6 is due to abnormal low-density measurements at 0300 LT. However, values at L16_14 and L2_si did increase at the end of the sampling period between 0005 and 0605 LT. The increase in brine was measured at L4_2 and L2_si, but the impact on thermal conductivity was only

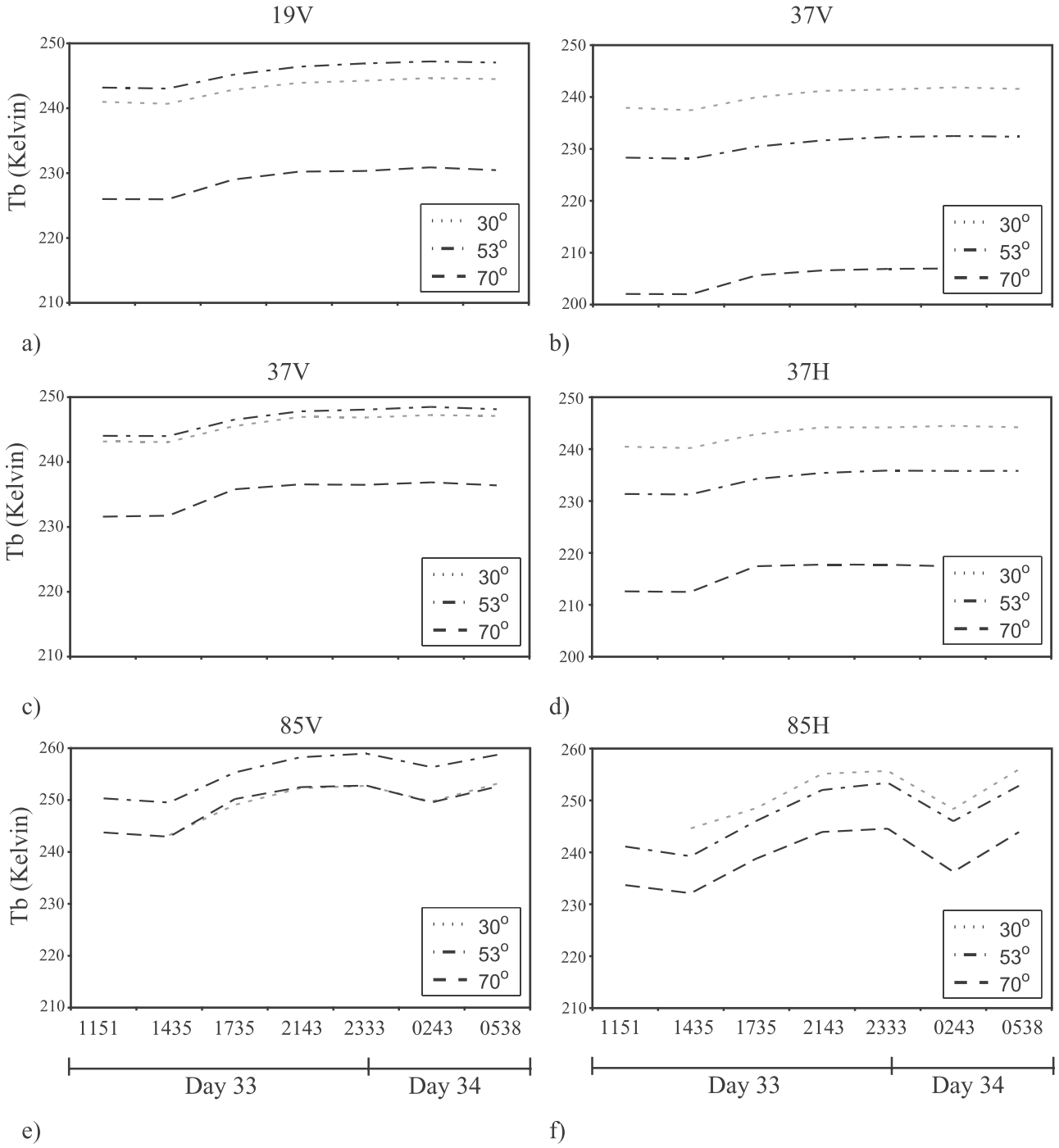

Figure 8. Temporal evolution of passive microwave brightness temperatures at vertical and horizontal polarizations for (a, b) 19 GHz, (c, d) 37 GHz, and (e, f) 85 GHz at 30, 53, and 70° of incidence angle.

noticed at L2_si with a slight increase between 0005 and 0605 LT. The effect of brine migration was mostly noticed through specific heat, which values at L4_2 peaked at 0300 LT (Figure 10b). As observed in thin snow, the thermal diffusivity decreased accordingly and reached its minimal value for the diurnal period.

[32] Thick snow grain growth rate was measured at 0.5 $mm^2\ d^{-1}$ by *Langlois et al.* [2007a] during the same period and location, and again this value is much lower than what we measured under the LPD at 2.3 $mm^2\ d^{-1}$ (Figure 11). The average temperature gradient 0.5 °C cm^{-1} during the duration of the sampling period, a value well above what is necessary to trigger temperature gradient metamorphism (~0.25 to 0.3 °C· cm^{-1} in work by *Colbeck* [1983] and *Sturm et al.* [2002]. The average vapor flux was $+1.94 \times 10^{-7}$ kg $m^{-2}\ s^{-1}$, higher than what was observed in thin snow. However, no physical data were available for thick snow to calculate a comparable vapor flux under a high-pressure system during this period. It is not surprising to have higher vapor flux values in thick snow covers due to

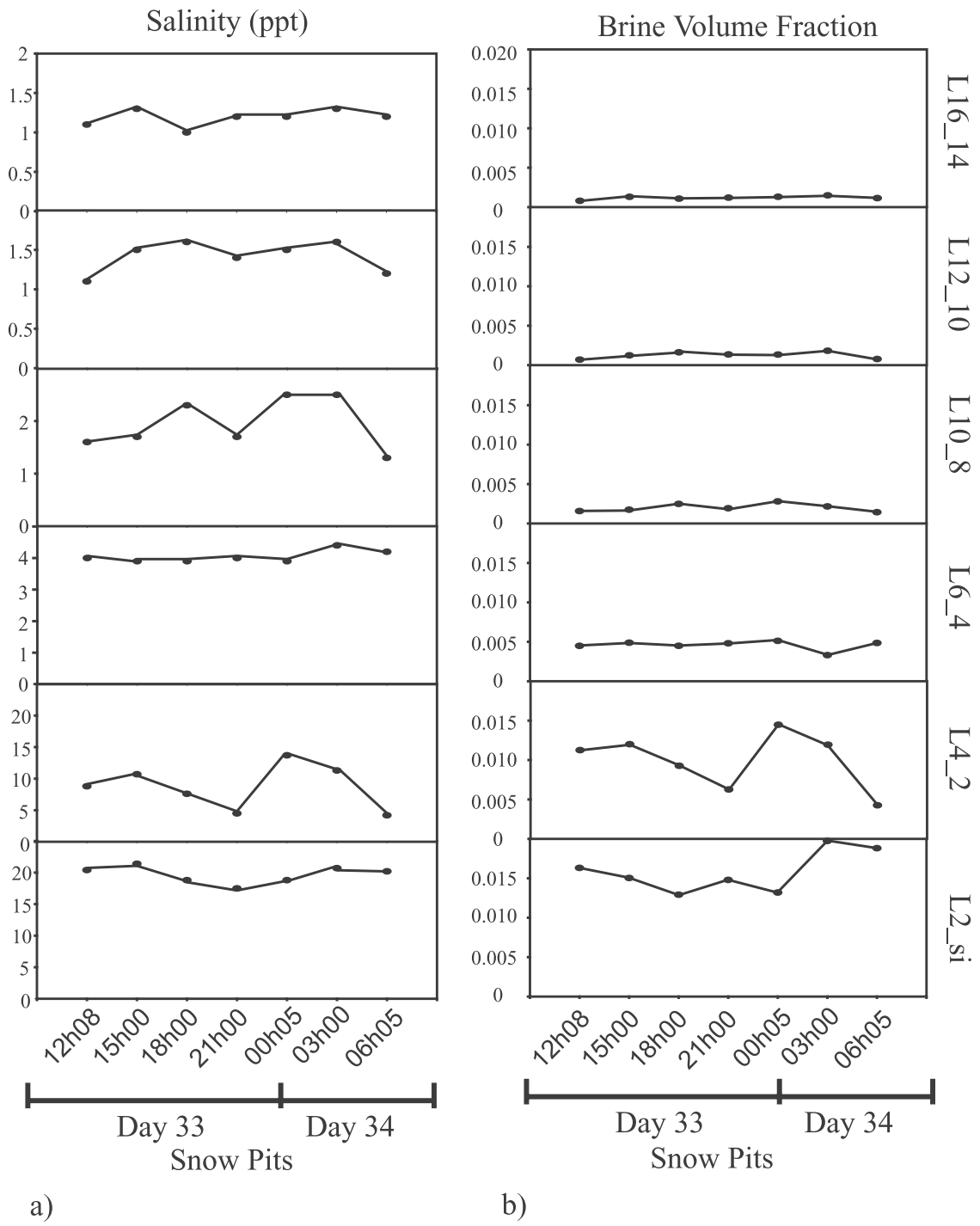

Figure 9. Temporal evolution of (a) salinity and (b) brine volume fraction for thick snow.

the greater amount of liquid water content [e.g., *Sturm and Johnson*, 1991; *Zhekamukhova*, 2004]. Owing to the high rate of grain growth, it can be assume that the LPD accelerated kinetic growth as observed in thin snow.

4.4. Snow Properties and T_b Variations

[33] During our sampling period, the temperature gradients remained linear, but more brine was available throughout the night with maximum air temperatures. The brine volume migration increased the permittivity and dielectric loss of the snow (Figure 5). The sensitivity of dielectric properties to increasing brine volume is well understood [e.g., *Tiuri et al.*, 1984; *Carsey*, 1992; *Eppler*, 1992], however no data set has yet shown that this migration could occur over a single diurnal period in the middle of the arctic winter.

[34] The microwave response did not appear to capture the observed increase in grain size, or at least it was masked by a corresponding increase in microwave emission due to increased brine volume. In either case the 19 and 37 GHz frequencies both showed a small increase in brightness

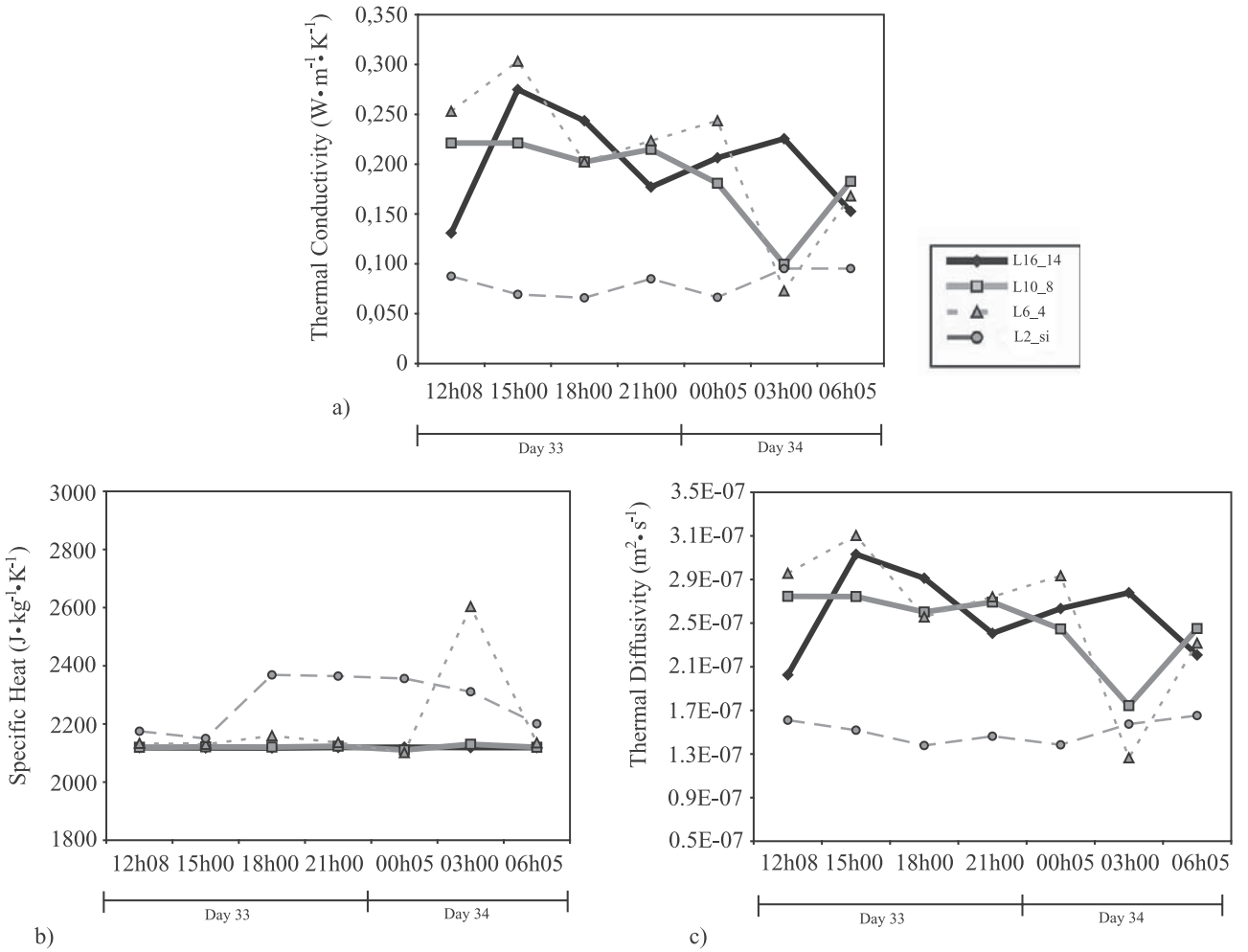

Figure 10. Temporal evolution of (a) thermal conductivity, (b) specific heat, and (c) thermal diffusivity for thick snow.

temperature over the diurnal period (Figures 8a–8d). Interestingly, there was a decrease of 4 K at 85 GHz vertically polarized and 8 K in the horizontal polarization at 0243 LT where the basal layer snow grains were at their maximum size. However, it is not likely that grain size explains the variations in 85 GHz Tbs since large grains were also present on the previous snowpit sampling (SP4) without measuring any changes in the 85 GHz brightness temperatures. However, coincident to this decrease in 85 GHz Tbs, we measured maximum values in salinity and brine volume (i.e., high permittivity and dielectric loss). The increasing permittivity decreased the emission contribution from the brine-rich basal layer that will decreases the overall brightness temperature [e.g., *Tiuri et al.*, 1984; *Walker and Goodison*, 1993; *Barber et al.*, 2003], confirming the high sensitivity of high frequencies to small increase in liquid water fraction and brine the snow.

5. Conclusion

[35] Our intention in examining this case study was to (1) document the geophysical, and thermodynamic response of snow over landfast first-year sea ice to a low-pressure system and (2) determine whether microwave radiometry could detect the changes imparted by this low-pressure system on the snow/sea ice geophysics. We showed that grain size changed over the study period at the bottom of both thin and thick snowpacks. We speculate that the LPD imparted a sufficiently strong effect on grain metamorphism that these systems could be considered as forcing episodic increases in grain size due to kinetic grain growth. The accumulation of several episodes of large rates of grain growth, from many LPDs, may be a significant seasonal feature of cyclones over snow covered sea ice due to the control this will have on radiative transfer in the spring. We note however that these grain size changes were not large enough to be detected by microwave radiometry directly. We speculate that this was because the absolute grain size increase had less of an effect that the concomitant increase in permittivity and loss (due to increased brine volume) at 19 and 37 GHz.

[36] It is difficult to compare both thin and thick snow from a passive microwave response perspective, as the incidence angles are not the same. However, at both low- and high-incidence angles (30° to 45° over thin; 55° to 70° over thick), 85 GHz did respond to increasing salinity and brine volume in the middle layers of the snowpack due to the combined influence of wind pumping (common under

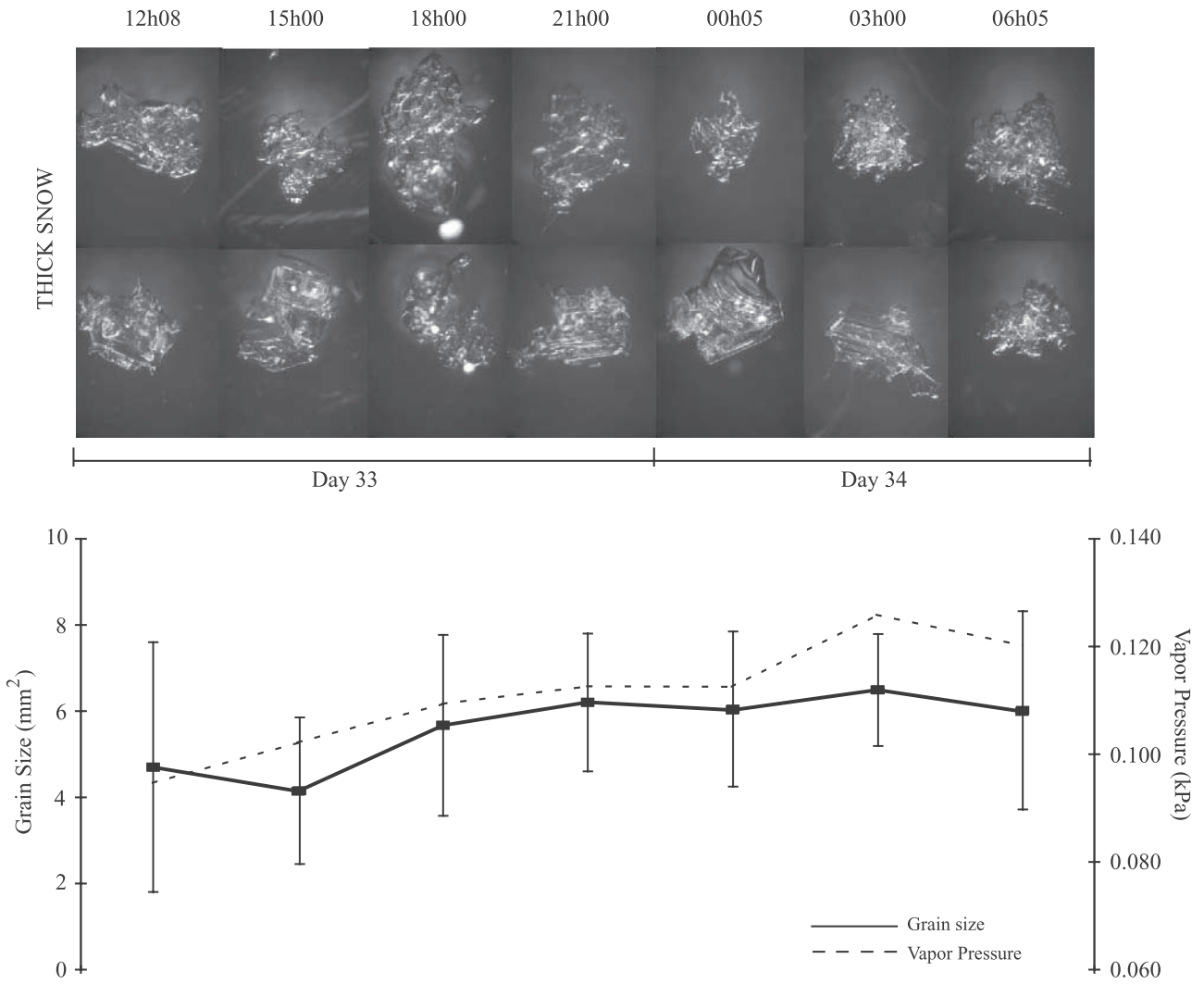

Figure 11. Temporal evolution of thick snow grain size and saturation vapor pressure.

low-pressure systems) and low-to-medium temperature gradient. Another limitation to the presented results is the absence of sea ice salinity values in the upper parts. The contributions of sea ice to the measured brightness temperatures are still not well understood and part of current work conducted in our lab. The relationship between penetration depth and brine volume (i.e., salinity and temperature) needs to be addressed seasonally throughout the sea ice and snow vertical profiles. The maximum brine volume was reached between 0300 and 0330 LT on day 34 where the brightness temperature at 85 GHz did decrease significantly at both polarizations. It was also shown that the snow grain growth rate is larger under the influence of a LPD. Rates of 1.28 and 2.3 mm^2 d^{-1} for thin and thick snow were measured between day 33 and 34 whereas previous work indicate rates of 0.25 and 0.5 mm^2 d^{-1}, respectively.

[37] It is an open question as to the possibility to detect LPD influences on the snow/sea ice geophysics at a satellite remote sensing scale. Other work recently submitted (A. Langlois et al., Estimation of snow water equivalent over first-year sea ice using AMSR-E and surface observations, submitted to *Remote Sensing of Environment*, 2007) showed that the atmospheric contribution on Tb was relatively small throughout the winter at all frequencies owing to the very dry conditions. Generally, the contribution at 85 GHz varies between 5 and 20 K depending on the cloud transmissivity. Throughout our experiment, this contribution varied between 3 and 9 K, within the range of what was observed at the SBR. Our in situ observations suggest that 85 GHz data can detect the increased grain size and or increased brine volume. We can assume that stronger cyclonic events might be needed to detect the changes in snow thermophysical properties from a passive microwave spaceborne instrument such as AMSR-E, which resolution is 12.5 km. Furthermore, the amplitude of the change might allow detection at lower frequencies such as 19 and 37 GHz. At this scale, the changes would still occur, but the spatial features (ridges, cracks, leads) might play a more important role in the microwave emission due to subpixel-scale effects. We see this research as providing a first step in understanding the role of cyclones in modifying snow and sea ice geophysics and the associated effects on gas, mass and energy transfer across the ocean–sea ice–atmosphere interface. As we move into the decades ahead we can expect cyclones to

play an increasingly important role in the climate of fast and marginal sea ice zones.

[38] **Acknowledgments.** This work was financially supported by grants for the CASES NSERC network, the Canada Foundation for Innovation (CFI), the Canada Research Chairs program, and the Polar Continental Shelf Project, each to D.G.B. The authors would like to thank the crew of the C.C.G.S. *Amundsen* for logistical support throughout the study and to Christina Blouw and Owen Owens from the University of Manitoba for tremendous support during the sampling period. Special thanks go to John Yackel from the University of Calgary for guidance and support throughout the experiment.

References

Albert, M. R. (2002), Effects of snow and firn ventilation on sublimation rates, *Ann. Glaciol.*, *35*, 510–514.

Armstrong, R. L., A. Chang, A. Rango, and E. Josberger (1993), Snow depths and grain size relationships with relevance for passive microwave studies, *Ann. Glaciol.*, *17*, 171–176.

Asmus, K., and C. Grant (1999), Surface Based Radiometer (SBR) Data Acquisition System, *Int. J. Remote Sens.*, *20*, 3125–3129.

Assur, A. (1958), Composition of sea ice and its tensile strength, in *Arctic Sea Ice*, *NRC Publ.*, vol. 598, pp. 106–138, Natl. Acad. Press, Washington, D. C.

Barber, D. G., and J. M. Hanesiak (2004), Meteorological forcing of sea ice concentrations in the southern Beaufort Sea over the period 1979 to 2000, *J. Geophys. Res.*, *109*, C06014, doi:10.1029/2003JC002027.

Barber, D. G., and E. F. LeDrew (1994), On the links between microwave and solar wavelengths interactions with snow covered first year sea ice, *Arctic*, *47*, 298–309.

Barber, D. G., and A. Thomas (1998), The influence of cloud cover on the radiation budget, physical properties and microwave scattering coefficient of first-year and multi-year sea ice, *IEEE Trans. Geosci. Remote Sens.*, *36*(1), 13 pp.

Barber, D. G., T. N. Papakyriakou, and E. F. LeDrew (1994), On the relationship between energy fluxes, dielectric properties, and microwave scattering over snow covered first-year ice during the spring transition period, *J. Geophys. Res.*, *99*(C11), 22,401–22,411.

Barber, D. G., S. P. Reddan, and E. F. LeDrew (1995), Statistical characterization of the geophysical and electrical properties of snow on landfast first-year sea ice, *J. Geophys. Res.*, *100*(C2), 2673–2686.

Barber, D. G., J. Iacozza, and A. Walker (2003), Estimation of snow water equivalent using microwave radiometry over Arctic first-year sea ice, *Hydrol. Processes*, *17*, 3503–3517.

Bartlett, M. G., D. S. Chapman, and R. N. Harris (2004), Snow and the ground temperature record of climate change, *J. Geophys. Res.*, *109*, F04008, doi:10.1029/2004JF000224.

Baunach, T., C. Fierz, P. K. Satyawali, and M. Schneebeli (2001), A model for kinetic grain growth, *Ann. Glaciol.*, *32*, 1–6.

Bergen, J. D. (1968), Vapour transport as estimated from heat flow in a rocky mountain snowpack, *Int. Assoc. Sci. Hydrol. Publ.*, *61*, 62–74.

Carsey, F. (1992), Remote sensing of ice and snow: review and status, *Int. J. Remote Sens.*, *13*, 5–11.

Clarke, G. K. C., D. A. Fisher, and E. D. Waddington (1987), Wind pumping: A potentially significant heat source in ice sheets, *IAHS Publ.*, *170*, 169–180.

Colbeck, S. C. (1980), Thermodynamics of snow metamorphism due to variations in curvature, *J. Glaciol.*, *26*, 291–301.

Colbeck, S. C. (1982), An overview of seasonal snow metamorphism, *Rev. Geophys.*, *20*(1), 45–61.

Colbeck, S. C. (1983), Theory of metamorphism of dry snow, *J. Geophys. Res.*, *88*(C9), 5475–5482.

Colbeck, S. C. (1989), On the micrometeorology of surface hoar growth on snow in mountainous area, *Boundary Layer Meteorol.*, *44*, 1–12.

Colbeck, S. C. (1993), The vapor diffusion coefficient for snow, *Water Resour. Res.*, *29*(1), 109–115.

Colbeck, S. C. (1997), A review of sintering in seasonal snow, *CRREL Rep. 97-10*, 11 pp., Cold Reg. Res. and Eng. Lab., Hanover, N. H.

Cox, G. F. N., and W. F. Weeks (1982), Equations for determining the gas and brine volumes in sea ice samples, *CRREL Rep. 82-30*, 20 pp., Cold Reg. Res. and Eng. Lab., Hanover, N. H.

Denoth, A. (1994), An electronic device for long-term snow wetness recording, *Ann. Glaciol.*, *19*, 104–106.

Denoth, A. (1989), Snow dielectric measurements, *Adv. Space Res.*, *9*, 233–243.

Déry, S. J., and M. K. Yau (2002), Large-scale mass balance effects of blowing snow and surface sublimation, *J. Geophys. Res.*, *107*(D23), 4679, doi:10.1029/2001JD001251.

Deser, C., J. E. Walsh, and M. S. Timlin (2000), Arctic sea ice variability in the context of recent wintertime atmospheric circulation trends, *J. Clim.*, *13*, 617–633.

Drinkwater, M. R., and G. B. Crocker (1988), Modeling changes in the dielectric and scattering properties of young snow-covered sea ice at GHz frequencies, *J. Glaciol.*, *34*(118), 274–282.

Drobot, S. D., and D. G. Barber (1998), Towards development of a snow water equivalence (SWE) algorithm using microwave radiometry over snow covered first-year sea ice, *Photogramm. Eng. Remote Sens.*, *64*, 414–423.

Ebert, E. E., and J. A. Curry (1993), An intermediate one-dimensional thermodynamic sea ice model for investigating ice-atmosphere interactions, *J. Geophys. Res.*, *98*(C6), 10,085–10,109.

Eppler, D. T. (1992), Passive microwave signatures of sea ice, in *Microwave Remote Sensing of Sea Ice*, *Geophys. Monogr. Ser.*, vol. 68, edited by F. Carsey, chap. 4, pp. 47–71, AGU, Washington, D. C.

Fisico, T. (2005), Meteorological Observations, in *CASES 2003-2004 Field Summary, CEOS-TEC-2004-09-01*, edited by A. Langlois et al., Sect. 3.3, pp. 70–110, Univ. of Manit., Winnipeg, Manit., Canada.

Flato, G. M., and R. D. Brown (1996), Variability and climate sensitivity of landfast Arctic sea ice, *J. Geophys. Res.*, *101*(C10), 25,767–25,777.

Frankenstein, G., and R. Garner (1967), Equations for determining the brine volume of sea ice from −0.5 to −22.9 degrees C, *J. Glaciol.*, *6*, 943–944.

Grenfell, T. C., and A. W. Lohanick (1985), Temporal variations of the microwave signatures of sea ice during late spring and early summer near Mould Bay NWT, *J. Geophys. Res.*, *90*(C3), 5063–5074.

Hanesiak, J., D. G. Barber, and G. M. Flato (1999), Role of diurnal processes in the seasonal evolution of sea ice and its snow cover, *J. Geophys. Res.*, *104*(C6), 13,593–13,603.

Hilmer, M., and P. Lemke (2000), On the decrease of arctic sea ice volume, *Geophys. Res. Lett.*, *27*(22), 3751–3754.

Hudak, D. R., and J. M. C. Young (2002), Storm climatology of the southern Beaufort Sea, *Atmos. Ocean*, *40*, 145–158.

Intergovernmental Panel on Climate Change (2001), *Climate Change 2001: The Scientific Basis, Contribution of Working Group I to the Third Assessment Report of the Intergovernmental Panel on Climate Change*, Cambridge Univ. Press, New York.

Izumi, K., and T. Huzioka (1975), Studies of metamorphism and thermal conductivity of snow, *Low Temp. Sci., Ser. A*, *33*, 91–102.

Langlois, A., C. J. Mundy, and D. G. Barber (2007a), On the winter evolution of snow thermophysical properties over landfast first-year sea ice, *Hydrol. Processes*, *21*, 705–716, doi:10.1002/hyp.6407.

Langlois, A., D. G. Barber, and B. J. Hwang (2007b), Development of a winter snow water equivalent algorithm using in-situ passive microwave radiometry over snow covered first-year sea ice, *Remote Sens. Environ.*, *106*(1), 75–88, doi:10.1016/j.rse.2006.07.018.

Matzler, C. (1987), Applications of the interaction of microwaves with natural snow cover, *Remote Sens. Rev.*, *2*, 259–387.

Maykut, G. A. (1978), Energy exchange over young sea ice in the central Arctic, *J. Geophys. Res.*, *83*(C7), 3646–3658.

McKay, C. P. (2000), Thickness of tropical ice and photosynthesis on a snowball Earth, *Geophys. Res. Lett.*, *27*(14), 2153–2156.

Oke, T. R. (1987), *Boundary Layer Climates*, 435 pp., Methuen, New York.

Perovich, D. K., and B. Elder (2001), Temporal evolution and spatial variability of the temperature of Arctic sea ice, *Ann. Glaciol.*, *33*, 207–212.

Poe, G., A. Stogryn, and A. T. Edgerton (1972), A study of the microwave emission characteristics of sea ice, *Final Tech. Rep. 1749R-2*, Aerojet Electrosyst. Co., Azusa, Calif.

Pollack, H. N., D. Y. Demezhko, A. D. Duchkov, I. V. Golovanova, S. Huang, V. A. Shchapov, and J. E. Smerdon (2003), Surface temperature trends in Russia over the past five centuries reconstructed from borehole temperatures, *J. Geophys. Res.*, *108*(B4), 2180, doi:10.1029/2002JB002154.

Pollard, D., and J. F. Kasting (2005), Snowball Earth: A thin-ice solution with flowing sea glaciers, *J. Geophys. Res.*, *110*, C07010, doi:10.1029/2004JC002525.

Rogers, R. R., and M. K. Yau (1989), *A Short Course in Cloud Physics*, 3rd ed., 290 pp., Butterworth-Heineman, New York.

Rothrock, D. A., and J. Zhang (2005), Arctic Ocean sea ice volumes: What explains its recent depletion?, *J. Geophys. Res.*, *110*, C01002, doi:10.1029/2004JC002282.

Serreze, M. C., J. E. Walsh, F. S. Chapin III, T. Osterkamp, M. Dyurgerov, V. Romanovsky, W. C. Oechel, J. Morison, T. Zhang, and R. G. Barry (2000), Observational evidence of recent change in the northern high-latitude environment, *Clim. Change*, *46*, 159–207.

Serreze, M. C., J. A. Maslanik, T. A. Scambos, F. Fetterer, J. Stroeve, K. Knowles, C. Fowler, S. Drobot, R. G. Barry, and T. M. Haran (2003), A record minimum arctic sea ice extent and area in 2002, *Geophys. Res. Lett.*, *30*(3), 1110, doi:10.1029/2002GL016406.

Sokratov, S. A., and N. Maeno (2000), Effective water vapor diffusion coefficient of snow under a temperature gradient, *Water Resour. Res.*, *36*(5), 1269–1276.

Sturm, M., and C. S. Benson (1997), Vapour transport, grain growth and depth-hoar development in the subarctic snow, *J. Glaciol.*, *43*(143), 42–59.

Sturm, M., and J. B. Johnson (1991), Natural convection in the subarctic snow cover, *J. Geophys. Res.*, *96*(B7), 11,657–11,671.

Sturm, M., J. Holmgren, M. König, and K. Morris (1997), The thermal conductivity of seasonal snow cover, *J. Glaciol.*, *43*(143), 26–41.

Sturm, M., J. Holmgren, and D. K. Perovich (2002), Winter snow cover on the sea ice of the Arctic Ocean at the Surface Heat Budget of the Arctic Ocean (SHEBA): Temporal evolution and spatial variability, *J. Geophys. Res.*, *107*(C10), 8047, doi:10.1029/2000JC000400.

Tiuri, M. E., A. H. Sihvola, E. G. Nyfors, and M. T. Hallikainen (1984), The complex dielectric constant of snow at microwave frequencies, *IEEE J. Oceanic Eng.*, *OE-9*(5), 377–382.

Trabant, D., and C. S. Benson (1972), Field experiments on the development of depth hoar, *Mem. Geol. Soc. Am.*, *135*, 309–322.

Ulaby, F. T., R. K. Moore, and A. K. Fung (1986), *Microwave Remote Sensing: Active and Passive*, vol. 3, pp. 1065–2162, Artech House, Norwood, Mass.

Wadhams, P., and N. R. Davis (2000), Further evidence of ice thinning in the Arctic Ocean, *Geophys. Res. Lett.*, *27*, 3973–3975.

Walker, A., and B. Goodison (1993), Discrimination of a wet snow cover using passive microwave satellite data, *Ann. Glaciol.*, *17*, 307–311.

Yackel, J., D. G. Barber, and T. N. Papakyriakou (2001), On the estimation of spring melt in the North Polynya using RADARSAT-1, *Atmos. Ocean*, *39*, 195–208.

Yen, Y.-C. (1981), Review of thermal properties of snow, ice and sea ice, *CRREL Rep. 81-10*, 27 pp., Cold Reg. Res. and Eng. Lab., Hanover, N. H.

Zhang, X., J. E. Walsh, J. Zhang, U. S. Bhatt, and M. Ikeda (2004), Climatology and interannual variability of Arctic cyclone activity, 1948–2002, *J. Clim.*, *17*, 2300–2317.

Zhekamukhova, I. M. (2004), Heat conduction and diffusion equation of steam in snow cover, *J. Eng. Phys. Thermophys.*, *77*(4), 816–820.

D. G. Barber, T. Fisico, A. Langlois, and T. N. Papakyriakou, Centre for Earth Observation Science, 440 Wallace Building, Clayton H. Riddell Faculty of Environment, Earth and Resources, University of Manitoba, Winnipeg, Manitoba, Canada R3T 2K1. (a.langlois2@usherbrooke.ca)